

# Estimation of Anisotropic Neutron Emission Spectrum Using Spatial Neutron Flux Profile Outside Vacuum Vessel<sup>\*)</sup>

Tomoki URAKAWA and Hideaki MATSUURA

*Department of Applied Quantum Physics and Nuclear Engineering,  
Kyushu University, 744 Motooka, Fukuoka 819-0395, Japan*

(Received 13 November 2020 / Accepted 9 March 2021)

It is known that emission spectrum of fusion products is anisotropically distorted from Gaussian distribution when fuel ion velocity distribution function is anisotropic non-Maxwellian distribution. Previously, anisotropic neutron emission has been measured in experiments with the Large Helical Device (LHD). In this study, as an application, a method for evaluating anisotropic neutron emission spectra by measuring the spatial profiles of the neutron flux is presented. Assuming beam-heated deuterium plasma in a JT-60SA class tokamak device, it was confirmed that the effect of neutron flux emission appears in the neutron flux spatial profile outside the vacuum vessel when the energy region to be measured is set to the high energy side. In addition, it was shown that the characteristic change of the anisotropic emission spectrum is reflected in the spatial profile of the neutron flux. Estimating the neutron anisotropic emission spectrum by this measurement method can lead to new proposals for fast ion diagnosis such as analysis of velocity distribution functions.

© 2021 The Japan Society of Plasma Science and Nuclear Fusion Research

Keywords: anisotropic neutron emission spectrum, neutron measurement, spatial neutron flux profile

DOI: 10.1585/pfr.16.2405064

## 1. Introduction

When fast ions are produced by fusion reaction and external heating, energetic non-Maxwellian component is formed in the ion velocity distribution function [1–6]. As a consequence of this non-Maxwellian component formation, the emission spectra of fusion-produced particles are distorted from the Gaussian distributions to high (low) energy sides [7]. Previously, measurement of the distorted neutron emission spectrum was used for fast ion diagnosis aimed at understanding the energetic ion characteristics in core plasma. Hence, it reflects characteristic of the non-Maxwellian component on the fuel ion velocity distribution function. In JET, the distortion component of neutron emission spectrum was measured to observe the fast ion distribution in third harmonic ICRF heating on deuterium beams, as well as  $\alpha$  “knock-on” process in DT plasma, by using high-resolution neutron spectroscopy [8–10].

The anisotropic non-Maxwellian component formed in the velocity distribution function leads to anisotropic distortion in the emission spectrum of fusion products. In the tangential deuterium-beam-injected DT plasma, the neutron emission spectrum is largely distorted from Gaussian to the higher (lower) energy side toward (opposite to) the NBI direction [11, 12]. In Ref. [13], the emission spectrum of neutrons produced by the  $D(d,n)^3\text{He}$  reactions in the proton-beam-injected deuterium plasma has been analyzed. In such plasmas, the anisotropic non-Maxwellian

component (knock-on tail) formed on the deuteron velocity distribution function due to nuclear elastic scattering (NES) [14] with the proton beam. The NES effect due to proton beam injection was actually observed using neutron measurement in the large helical device (LHD)-based deuterium plasma experiments [15]. The anisotropic neutron emission is also caused by the differential cross-section of the  $D(d,n)^3\text{He}$  reaction [16]. Higher energy beam injection induces the emission of neutrons produced by  $D(d,n)^3\text{He}$  reaction toward NBI direction.

The large anisotropy of neutron emission caused was actually observed in the LHD-based deuterium plasma experiments using tangential NBI. It was reported that the anisotropic neutron emission spectrum during NBI heating appears as a difference in the neutron flux measured by neutron flux monitor which installed near the equatorial port and center axis, or neutron activation system which installed at outside port and lower vertical port [17, 18]. This difference was used to ascertain the neutron emission anisotropy and was used for fast ion diagnostic. In addition to the observation of anisotropic neutron emission on a fusion reactor scale, the above experiments in LHD suggest that their anisotropy affects the spatial distribution of the neutron flux. Therefore, there is a possibility to estimate the anisotropic neutron emission spectrum in detail based on the measurement the spatial neutron flux profile outside the vacuum vessel. Especially in beam-injected deuterium plasma experiments conducted in LHD and JT-60SA [19], this measurement can be realized, because neutron produced by  $D(d,n)^3\text{He}$  reaction provide sufficient anisotropy.

author's e-mail: urakawa-0804@nucl.kyushu-u.ac.jp

<sup>\*)</sup> This article is based on the presentation at the 29th International Toki Conference on Plasma and Fusion Research (ITC29).

This leads to the proposal a new fast ion diagnostic method such as analysis of velocity distribution functions, which will be a much easier method technically than that using a neutron spectroscopy. It is first necessary to confirm whether the neutron flux measured outside the vacuum vessel retains sufficient information to reproduce the neutron emission spectrum in plasma.

In this study, a method for evaluating anisotropic neutron emission spectra by measuring the spatial profiles of the neutron flux is presented. We evaluated the correlation between the anisotropic neutron emission spectra and the spatial profiles of the neutron flux outside the vacuum vessel. As an example of anisotropic fast-ion generation, proton-beam-injected deuterium plasma was assumed and the neutrons produced by the  $D(d,n)^3\text{He}$  reaction were measured. The neutron transport model was simulated JT-60SA class tokamak device. Section 2 describes the method of calculation and the model for transporting neutrons. Results and discussion are shown in section 3. Finally, the concluding remarks are given in Section 4.

## 2. Analysis Model

### 2.1 Double differential neutron emission spectrum

In this study, we simulated a distorted neutron emission spectrum from the Gaussian distribution by superimposing two Gaussian distribution. In addition, neutron produced by  $D(d,n)^3\text{He}$  fusion reaction is assumed. The double differential neutron emission spectrum is written as follows:

$$\frac{d^2 N_n}{dE d\Omega_{lab}}(E, \theta_n) = \frac{S}{n^{1/2}} \left[ \frac{1 - \alpha}{\Delta_{NG}} \exp\left(-\left(\frac{E - E_{NG}^0}{\Delta_{NG}}\right)^2\right) + \frac{\alpha}{\Delta_G} \exp\left(-\left(\frac{E - E_G^0}{\Delta_G}\right)^2\right) \right]. \quad (1)$$

Here,  $\Delta_{G(NG)}$  is

$$\Delta_{G(NG)} = \sqrt{\frac{4m_n E_{G(NG)}^0 T_{G(NG)}}{m_{^3\text{He}} + m_n}}, \quad (2)$$

$E_{NG}^0$  shows the average energy of Gaussian component introduced to simulate the distortion component

$$E_{NG}^0(\theta_n) = \frac{-0.25 \tanh(\kappa(2\theta_n - \pi))}{\tanh(-\kappa\pi)} + 2.52. \quad (3)$$

Here,  $E_{NG}^0$  is a function of emission direction  $\theta_n$  to simulate the anisotropy of the distortion component. Where  $S$  is neutron total emission rate,  $\alpha$  is intensity ratio of Gauss component to total emission,  $E_G^0$  is average energy of Gaussian component (2.45 MeV),  $m_{(^3\text{He})}$  is neutron ( $^3\text{He}$ ) mass and  $T_{G(NG)}$  is temperature of Gauss (distortion) component.  $\theta_n$  represents the angle between the direction of the emitted neutron and that of the toroidal axis in the laboratory system.  $\kappa$  is a coefficient that determines the direction dependence of the average energy of distortion component. Figure 1 shows the direction dependence

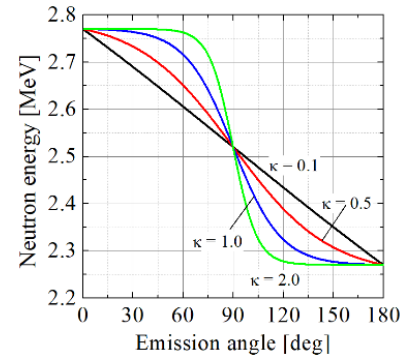


Fig. 1  $E_{ng}$  emission direction dependence when  $\kappa = 0.1, 0.5, 1.0$  and 2.0.

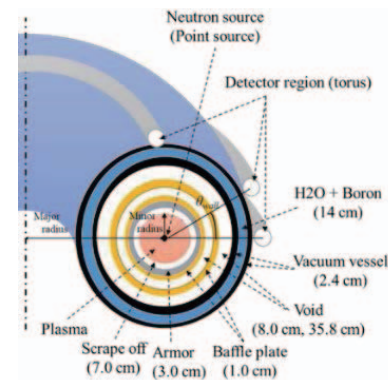


Fig. 2 The model used for MVP neutron transport calculations assuming the JT60-SA class tokamak device.

of the  $E_{NG}^0$  at various  $\kappa$ . When  $\kappa$  is around 1.0, the direction dependence of the  $E_{NG}^0$  reflects the characteristics of tanh. On the other hand, when  $\kappa = 0.1$ , the average energy and the emission direction are proportional.

### 2.2 Neutron transport calculation

Figure 2 shows the computational schema of the 3D-torus form with the neutron flux measurement region which placed outside of vacuum vessel (VV). In this study, the JT-60SA class tokamak device (major radius 2.97 m, minor radius 1.16 m) is assumed.  $\theta_{wall}$  represents poloidal angle, which is the angle between the measurement regions and the equatorial direction (See Fig. 2). In this study, the multiple torus form (minor radius 10 cm) neutron measurement regions were placed along the vacuum vessel and were wrapped around the tokamak device. These measurement regions were arranged with an equal angle width ( $9^\circ$ ) in the range of  $0^\circ \leq \theta_{wall} \leq 90^\circ$ , and evaluate the poloidal angle dependence of the neutron flux. Table 1 shows the layer structure from the core plasma to the VV and its thickness [19].

The neutron flux in the measurement regions is calculated using the Monte Carlo transport code MVP [20] with reference to the JENDL-4.0 [21] nuclear data library. The neutron emission spectra were used as the point source in

Table 1 the layer structure.

layer	Thickness [cm]	Component
Scrape off	7.0	-
Armor	3.0	F82H
Baffle plate	1.0	SS316L
Void	8.0	-
Baffle plate	1.0	SS316L
Void	35.8	-
Vacuum vessel	2.4	SS316L
H <sub>2</sub> O + Boron	14.0	H <sub>2</sub> O (99.22%) - Boron (0.78%)
Vacuum vessel	2.4	SS316L

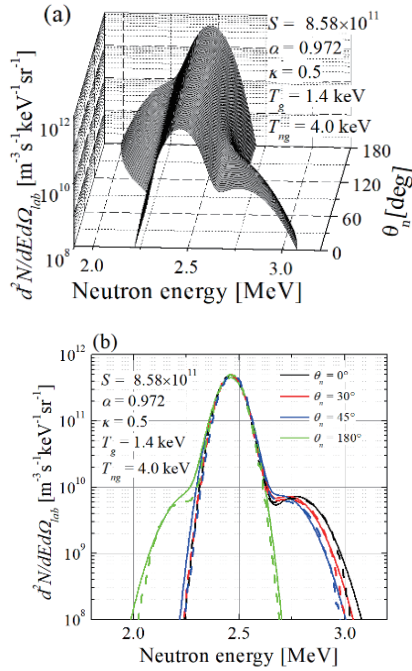


Fig. 3 Double differential neutron emission spectrum: (a) all emission directions and (b) in the directions of  $\theta_n = 0^\circ, 30^\circ, 45^\circ$  and  $180^\circ$ .

the neutron transport calculations, which is placed in the center of plasma. For neutron sources, the angle and energy mesh sizes are  $\Delta\theta = 3^\circ$ ,  $\Delta E = 5$  keV, respectively.

### 3. Result and Discussion

#### 3.1 Anisotropic neutron emission spectrum

In this section, we describe the characteristics of the double differential neutron emission spectrum which was calculated using eq.(1). First, we reproduce the double differential neutron emission spectrum (deuteron density  $n_d(0) = 10^{19} \text{ m}^{-3}$ , electron temperature  $T_e(0) = 2$  keV, proton beam energy and power  $E_{NBI} = 200$  keV,  $P_{NBI} = 33$  MW) presented in Ref. [13]. We discuss the validity of the two Gauss distribution superposition models. In Fig. 3, the double differential neutron emission spectrum was shown as a function of both the energy and the direction ((a) all emission direction, (b) in the direction of  $\theta_n = 0^\circ, 30^\circ, 45^\circ$  and  $180^\circ$ ). The solid lines in Fig. 3 (b) shows the neutron emission spectra which were calculated using eq. (1). The broken lines show the neutron emission

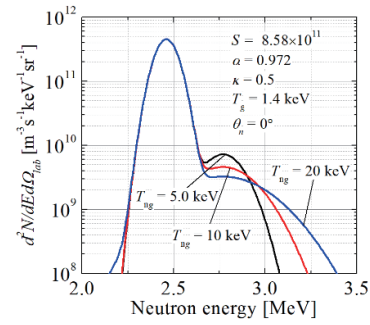


Fig. 4 Double differential neutron emission spectra at the  $\theta_n = 0^\circ$  when  $T_{ng} = 4.0, 10, 20$  keV.

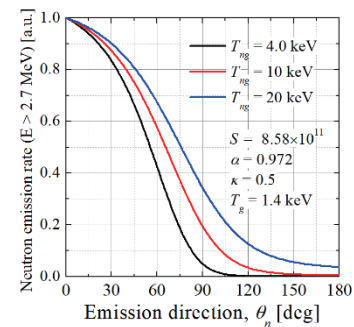


Fig. 5 Double differential neutron emission spectra at the  $\theta_n = 0^\circ$  when  $T_{ng} = 4.0, 10, 20$  keV.

spectra presented in Ref. [13]. When reproducing, each parameter is as follow;  $S = 8.58 \times 10^{11} \text{ m}^{-3} \text{ s}^{-1}$ ,  $\alpha = 0.972$ ,  $\kappa = 0.5$ ,  $T_g = 1.4$  keV,  $T_{ng} = 4.0$  keV. In Fig. 3 (a), it can be confirmed that the double differential neutron emission spectrum reproduces the characteristics of it presented in Ref. [13]. When comparing each solid line and broken line in Fig. 3 (b), the energy regions of the distortion components are approximately the same in each emission direction. However, the strength of the distortion component at  $\theta_n = 180^\circ$  is overestimated.

Figure 4 shows double differential neutron emission spectra at  $\theta_n = 0^\circ$  when  $T_{ng} = 4.0, 10, 20$  keV. The distortion component spreads to the high energy side as  $T_{ng}$  increase. This is because the half width increases based on eq. (2). When  $T_{ng} = 20.0$  keV, the total number of neutrons emitted with energies exceeding 2.7 MeV increases by a factor of 1.19 compared to the case where  $T_{ng} = 4.0$  keV. Figure 5 shows the total number of neutrons emitted with energies more than 2.7 MeV as a function of emission direction when  $T_{ng} = 4, 10, 20$  keV. The spread of the distortion component toward the high energy side increases the emission rate of neutrons with energies more than 2.7 MeV in all emission direction. Therefore, the anisotropy of the neutron emission rate is relaxed as  $T_{ng}$  increases.

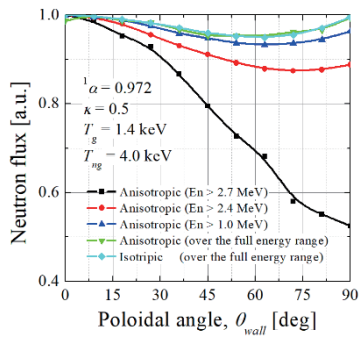


Fig. 6 Neutron flux spatial profile as a function of poloidal angle, which evaluated using anisotropic emission spectrum ( $T_g = 1.4$  keV,  $T_{ng} = 4.0$  keV,  $\kappa = 0.5$  and  $\alpha = 0.972$  are assumed).

### 3.2 Anisotropic neutron emission spectra estimation using the spatial neutron flux profile outside vacuum vessel

In this section, we describe the characteristics of the spatial neutron flux profile outside the vacuum vessel when using the anisotropic neutron source. Figure 6 shows the spatial neutron flux profile outside the vacuum vessel which is evaluated using double differential neutron emission spectrum in Fig. 2 ( $T_g = 1.4$ ,  $T_{ng} = 4.0$ ,  $\kappa = 0.5$  and  $\alpha = 0.972$ ). The neutron flux profile obtained by using the isotropic neutron source (mono energy, 2.45 MeV) is also shown. For isotropic neutron source, the neutron flux is highest around  $\theta_{wall} = 0^\circ$  and  $90^\circ$ . This is considered a geometric effect. In the case of anisotropic neutron source, the neutron flux profile differs depending on the energy range to be measured. When measuring a total neutron flux or neutron flux with energies more than 1.0 MeV, the neutron flux profile is the same as that of isotropic neutron emission. In other word, the effect of anisotropic neutron emission cannot be confirmed. On the other hand, when measurement energy region is set to the higher energy side ( $E_n > 2.4$  or 2.7 MeV), the effect of anisotropic neutron emission on the neutron flux spatial profile appears. The neutron flux near the equatorial port ( $\theta_{wall} = 0^\circ$ ) is about 50% larger than of that measured above the tokamak apex ( $\theta_{wall} = 90^\circ$ ) due to anisotropic neutron emission when measuring neutron flux with energies more than 2.7 MeV. In addition, this confirmed that the emission direction distributions of neutron emission rate shown in Fig. 5 and the spatial neutron flux profile outside the vacuum vessel have the same tendency. Therefore, the spatial neutron flux profile outside the vacuum vessel holds sufficient information on the anisotropic neutron emission spectrum. However, the spatial neutron flux profile is less anisotropy than the neutron emission rate directional distribution because the size of device is large enough to diffuse neutrons.

Figure 7 shows the spatial neutron flux profile which is evaluated using the anisotropic emission spectra when  $T_{ng} = 4.0, 10, 20$  keV. It is confirmed that the difference

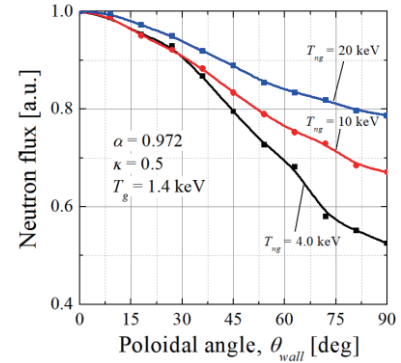


Fig. 7 Neutron flux spatial profile evaluated using anisotropic emission spectra when  $T_{ng} = 4.0, 10, 20$  keV.

in the anisotropic neutron emission spectrum appears as the difference in the spatial neutron flux profile outside the vacuum vessel. When  $T_{ng}$  increases, the effect on the neutron flux profile is mitigated. This is because the emission rate of high energy neutrons ( $E_n > 2.7$  MeV) increased in all emission direction in Fig. 5. This result indicates that differences in neutron flux profile can lead to the estimation of anisotropic neutron emission spectra. When the spread of the distortion component can be measured, it may lead to the diagnostic of the energy range of the non-Maxwellian component formed in the velocity distribution function.

## 4. Conclusion Remarks

In this study, we presented a method for evaluating anisotropic neutron emission spectra by measuring the spatial profiles of the neutron flux. It was assumed that the neutrons were produced by the  $D(d,n)^3\text{He}$  reaction in proton-beam injected deuterium plasma. The neutron transport model was simulated JT-60SA class tokamak device. We evaluated the correlation between the neutron emission spectra and the spatial neutron flux profiles outside the vacuum vessel. Due to the anisotropic neutron emission spectrum, the neutron flux on the tokamak equatorial plane is the highest, which has the attenuation that decreases toward the apex. When the measurement energy region is fixed at above 2.7 MeV, the neutron flux on the tokamak equatorial plane was about 50% higher than that at the torus apex and the attenuation distribution was clearly appeared. It is observed that the neutron flux profile reflects the characteristic of anisotropic neutron emission spectra. When the energy region of distortion component expands, the differences also appeared in the neutron flux profile. Therefore, it can be possible to estimate the characteristics of the anisotropic neutron emission spectra by measuring this profile, which can be used to analyze the velocity distribution function of the fast ions.

In this study, we assumed proton-beam-injected deuterium plasma, which formed the anisotropic non-

Maxwellian component on the deuteron velocity distribution function due to nuclear elastic scattering with the proton beam. Since the effect on the neutron flux spatial distribution could be confirmed under the conditions, this measurement method would be more feasible when large anisotropic neutron emission such as the deuteron-beam-injected deuterium plasma.

In this study, the double differential neutron emission spectrum was simulated by superimposing two Gaussian distributions. It is necessary to evaluate the neutron emission spectrum based on the velocity distribution function of fuel ions. Moreover, in this study, we only confirm the effect of anisotropic neutron emission on the neutron flux spatial profile. In the future, it will be necessary to consider the selection of a neutron detector (e.g., radiation foil with a threshold value) that can identify high-energy neutrons suitable for this measurement method. Finally, the actual fusion reactor is elliptical, and even when neutrons are emitted isotropically, the neutron wall load shows a distribution (specific to each tokamak device). Therefore, in order to use this diagnostic method, a simulation is required in advance for each device.

- [1] J.G. Cordey and M.J. Houghton, Nucl. Fusion **13**, 215 (1973).
- [2] T.H. Stix, Nucl. Fusion **15**, 737 (1975).
- [3] M. Yamagiwa, T. Takizuka and Y. Kishimoto, Nucl. Fusion **27**, 1773 (1987).
- [4] M. Nocente, G. Gorini, J. Källne and M. Tardocchi, Nucl. Fusion **51**, 063011 (2011).
- [5] Ya.I. Kolesnichenko, Nucl. Fusion **20**, 727 (1980).
- [6] H. Matsuura and Y. Nakao, Phys. Plasmas **13**, 062507 (2006).
- [7] H. Matsuura and Y. Nakao, Phys. Plasmas **16**, 042507 (2009).
- [8] L. Ballabio, G. Gorini and J. Källne, Phys. Rev. E **55**, 3358 (1997).
- [9] J. Källne *et al.*, Phys. Rev. Lett. **85**, 1246 (2000).
- [10] C. Hellesen *et al.*, Nucl. Fusion **50**, 022001 (2010).
- [11] H. Matsuura and Y. Nakao, J. Plasma Fusion Res. SERIES **9**, 48 (2010).
- [12] S. Sugiyama *et al.*, Phys. Plasmas **24**, 092517 (2017).
- [13] H. Matsuura *et al.*, IEEE Trans. Plasma Sci. **46**, 6 (2018).
- [14] J.J. Devaney and M.L. Stein, Nucl. Sci. Eng. **46**, 323 (1971).
- [15] H. Matsuura *et al.*, Nucl. Fusion **60**, 066077 (2020).
- [16] M. Drosig and O. Schwerer, Production of monoenergetic neutrons between 0.1 and 23 MeV: neutron energies and cross-sections, Handbook of Nuclear Activation Data (Vienna: IAEA) STI/DOC/10/273, ISBN 92-0-135087-2 (1987).
- [17] T. Nishitani *et al.*, IEEE Trans. Plasma Sci. **47**, 12 (2018).
- [18] S. Sugiyama *et al.*, Nucl. Fusion **60**, 076017 (2020).
- [19] A.M. Sukegawa *et al.*, Fusion Eng. Des. **82**, 2799 (2007).
- [20] Y. Nagaya, K. Okumura, T. Mori and M. Nakagawa, JAERI 1348 (2005).
- [21] K. Shibata *et al.*, J. Nucl. Sci. Technol. **48**, 1 (2011).